Front. Earth Sci. 2018, 12(1): 17–23
https://doi.org/10.1007/s11707-016-0618-8

RESEARCH ARTICLE

Factors that affect coseismic folds in an overburden layer

Shaogang ZENG[1,2], Yongen CAI (✉)[1]

1 Department of Geophysics, Peking University, Beijing 100871, China
2 Deep Water Exploration Group, Research Institute, CNOOC Nanhai East Petroleum Bureau, Guangzhou 510200, China

Abstract Coseismic folds induced by blind thrust faults have been observed in many earthquake zones, and they have received widespread attention from geologists and geophysicists. Numerous studies have been conducted regarding fold kinematics; however, few have studied fold dynamics quantitatively. In this paper, we establish a conceptual model with a thrust fault zone and tectonic stress load to study the factors that affect coseismic folds and their formation mechanisms using the finite element method. The numerical results show that the fault dip angle is a key factor that controls folding. The greater the dip angle is, the steeper the fold slope. The second most important factor is the overburden thickness. The thicker the overburden is, the more gradual the fold. In this case, folds are difficult to identify in field surveys. Therefore, if a fold can be easily identified with the naked eye, the overburden is likely shallow. The least important factors are the mechanical parameters of the overburden. The larger the Young's modulus of the overburden is, the smaller the displacement of the fold and the fold slope. Strong horizontal compression and vertical extension in the overburden near the fault zone are the main mechanisms that form coseismic folds.

Keywords ground deformation, coseismic fold, blind thrust fault, finite element method

1 Introduction

Some earthquake fault ruptures may not reach the ground surface. The 1994 Mw 6.7 earthquake in Northridge, California, was caused by a previously undiscovered blind thrust fault (https://en.wikipedia.org/wiki/1994_Northridge_earthquake), and the 2013 Lushan (China) Mw 7.0 earthquake is generally considered a blind fault event because no ground surface rupture has been found (Xu et al., 2013). Seismic reflection profiles have revealed the presence of active blind faults (Shaw and Shearer, 1999; Ishiyama et al., 2011). The thickness of an overburden layer above a blind fault can range from tens of meters in mountainous areas to hundreds of meters or more in river valleys and on the Loess Plateau (Miller and Xia, 1998; Shaw and Shearer, 1999; Ishiyama et al., 2011).

Coseismic folds induced by fault rupture have been found in many earthquake areas, and they have received widespread attention from geologists and geophysicists (Lewis et al., 2013; Zuluaga et al., 2014; Qayyum et al., 2015; Walker et al., 2015). These folds have garnered considerable academic interest, and they have been recognized as critical for assessing seismic hazards. There are two types of coseismic folds. In the first type, which includes the Lemhi fault in east-central Idaho, fault rupture reaches the ground surface and forms distinct fault scarps along Quaternary surface ruptures (Turko and Knuepfer, 1991). The second type, which includes the folds occurring in the 2013 Mw 7.0 Lushan (China) earthquake (Xu et al., 2013), is caused by a blind fault with overburden layers and fault ruptures do not extend to the surface. The former are generally called "fault scarps". For distinction, we call the latter "overburden folds" in this study because they are characterized by localized folding of the ground. These two types of folds have different deformation patterns that can be classified as fault-propagation folds and shear fault-bend folds in structural geology. The amounts of stratum shortening and uplift, as well as the fault slip rate, can be approximately inferred from the fault-related folds (Shaw and Suppe, 1996; Hubert-Ferrari et al., 2007; Hughes et al., 2014). Fault-propagation folds and fault-bend folds are often studied using kinematic methods (Suppe et al., 1992; Brandes and Tanner., 2014), including numerical modeling and experiments.

Many theoretical and numerical studies of seismic folds have been conducted. Suppe (1983) presented an idealized geometric description of two-dimensional fault-bend folding and demonstrated the quantitative use of the theory

Received January 24, 2016; accepted September 18, 2016

E-mail: yongen@pku.edu.cn

to identify subsurface map-scale structures in fold-and-thrust belts. Lin and Stein (1989) modeled the 1987 Whittier Narrows Mw 6.0 earthquake, which occurred on a blind fault and uplifted a Quaternary fold, using a simple dislocation model in an elastic half-space. The numerical results of the model fit the geodetic data well. Shaw and Suppe (1996) studied the fault-bend folds in the Los Angeles basin and revealed the size and slip rates of several blind thrust faults. Roering et al. (1997) developed numerical models to study "co-seismic deformation associated with thrust-related anticlines" and determine "why blind thrust faults do not propagate to the Earth's surface". Johnson and Johnson (2002) used a mechanical model of forced folding to investigate the influences of various parameters on the theoretical fold form. They found that the degree of anisotropy in the cover largely influenced the geometry of the forced fold. Hardy and Finch (2006) used a discrete element model (DEM) to investigate the influence of sedimentary cover strength on the development of basement-involved fault-propagation folds. They found that uniformly weak cover best promotes the development of folds, and layered heterogeneous covers of different strengths promote the development of more complex and variable fold forms. Recently, Hughes et al. (2014) constructed a series of discrete element mechanical models to investigate the roles and relative importance of various ranges of geometric and mechanical factors in the development of fault-related folds. They found that increased effective friction along the upper detachment and restricted motion at the foreland wall had the largest influences on fault-propagation folds. Some of the above mentioned numerical results were based on fault dislocation models in an elastic half-space, while others were based on DEMs. These models fail to consider the effects of fault zone thickness and heterogeneous materials on the deformation and stress fields.

Some laboratory experiments have successfully simulated the processes of fold formation and development. Bernard et al. (2007) analyzed the kinematics of fault tip folding at the front of a fold-and-thrust wedge using a sandbox experiment and proposed a method of determining the fold kinematics from the growth strata geometry and deformed geomorphic markers. Their findings suggest that fold kinematics can be described using a simple analytical formulation that assumes the velocity field is a linear function of depth and horizontal distance. Galuppo et al. (2016) used sandbox analogue models to investigate the fracture pattern evolution in fault-related anticlines, e.g., fault-propagation and fault-bend folds. These slow loading experiments may reveal some kinematic features of the formation processes of the folds; however, the natural factors used in these models are difficult to quantify and scale.

Collectively, the majority of the above kinematic studies have explained various long-term deformation features of fold-related regional-scale structures from a kinematic perspective. However, the overburden folds that are directly formed during the earthquake process are seldom studied in dynamics. In this paper, we investigate the factors that affect overburden folds and the associated fold formation mechanisms using a conceptual mechanical model with fault zones and heterogeneous materials. The model is based on elastic theory and the finite element method.

2 Numerical model

In mechanics, earthquakes are often considered unstable dynamic processes of stress release induced by sudden softening of or material damage to a fault zone. From this point of view, they can be simulated by decreasing the mechanical parameters of fault zone materials under the control of a tectonic stress field. In this paper, a 2-D conceptual finite element model (Hu et al., 2009; Zhou et al., 2009) with a fault zone and linear elastic constitutive relationship (Fig. 1) is used to study ground surface deformation and coseismic overburden folding caused by a blind thrust fault.

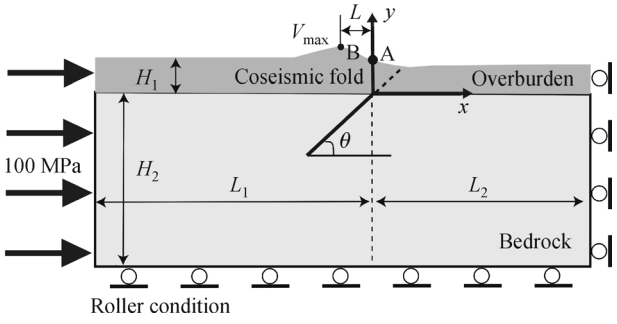

Fig. 1 Sketch of the numerical model and seismic overburden fold.

The fluctuation in the ground surface represents a coseismic fold caused by blind thrust fault slip (not to scale). H_1 indicates the thickness of an overburden layer, and θ is the fault dip angle. The original coordinate system is located at the upper fault tip, and the x and y-axes are in the horizontal and vertical directions, respectively. The bedrock thickness H_2, hanging wall width L_1, and footwall width L_2 are 120 km, 200 km, and 150 km, respectively. Point A is vertical projection of the upper fault tip on the ground surface and Point B is located at the fold crest.

The overall dimensions of the model are 350 km wide and 120 km deep. The thickness of the fault zone is 1 m, and the fault width along the slope is 25 km. A typical tectonic stress of 100 MPa (Donald and Gerald, 2001) is applied to the left boundary to create an initial field of tectonic stress without considering the effect of gravity, as it does not induce new deformation during coseismic activity. The ground surface is free, and the other boundaries are supported by rollers.

The dip angles and overburden thicknesses are 30°, 45°, 60° and 0 m, 10 m, 500 m, respectively. Additionally, the Young's modulus and Poisson's ratio in the overburden are regarded as uniform and isotropic, and they are set at 2.12×10^6 MPa (on the order of soil), 2.12×10^8 MPa (on the order of sands or soft rocks), 2.12×10^{10} MPa (on the order of some rocks) and 0.34, 0.40, 0.46, respectively (Shi, 1994; Yang et al., 2003). The Young's modulus and Poisson's ratio in the bedrock (see Fig. 1) are set at 83.7 GPa and 0.25, respectively, corresponding to a shear modulus of 33.48 GPa. The fault zone is considered a transversely isotropic material with five independent parameters: Young's modulus $\boldsymbol{E_1}$ and Poisson's ratio $\boldsymbol{v_1}$ along the fault slope and Young's modulus $\boldsymbol{E_2}$, Poisson's ratio $\boldsymbol{v_2}$ and shear modulus $\boldsymbol{G_2}$ in the normal direction of the fault. Before fault slip, these parameters are set to those of the bedrock, except the shear modulus $\boldsymbol{G_2}$ of 20 GPa, which is smaller than that outside the fault zone (Gudmundsson, 2004).

3 Numerical results

3.1 Typical deformation features of the ground surface and overburden folds

To understand some typical features of coseismic deformation and overburden folding caused by a blind thrust fault, a conceptual model with an overburden of 80 m and a fault with a dip of 30° is established. The simulation results near the upper fault tip are shown in Fig. 2.

Typical thrust deformation is induced by fault slip, the hanging wall thrusting up and the foot wall subducting down along the fault (Figs. 2(a) and 2(b)) to create a fold on the ground surface (Suppe, 1983). The dip angle of the front slope, pointing out the moving direction of the hanging wall, is larger than that of the back slope. Thus, the front slope can be used to determine the dip direction of the hanging wall. The strains in Figs. 2(c) and 2(d) show that the overburden is under strong compression and extension in the horizontal and vertical directions near the upper tip of the fault, respectively. These displacement and strain features can be used to explain the formations of overburden folds found in the field surveys (Bray, 2001; Chen et al., 2008; Yu et al., 2010). To better understand the details of these features, the surface displacements are plotted in Figs. 2(e) and 2(f). The maximum displacements are mainly concentrated near the upper fault tip. In Figs. 2 (e) and 2(f), the results of the simulations that include 80 m of overburden are considerably different from those of simulations with no overburden (dashed line). In the former, the maximum vertical displacement of 0.424 m occurs at point B, approximately 41 m from the vertical projection of the upper fault tip at the surface (point A in Fig. 1). Overburden folds induced by thrust faults were observed in North Yinxiu, Hongkou, and Chenjiaba during the 2008 Wenchuan Mw 8.0 earthquake (Chen et al., 2008; Yu et al., 2010). In the latter model (without overburden), the maximum horizontal and vertical displacements are 0.466 m and 0.349 m, respectively. Both of these values occur at the fault trace, and a fault scarp is created. For the same amount of fault zone damage or the same earthquake magnitude, the overburden fold is higher than the fault scarp. The result implies that the overburden amplifies vertical deformation and that the fault scarp is steep compared to the overburden fold. Without overburden, the fault scarp exhibits the same dip as the fault, while the overburden fold may occur in the opposite direction as that of the fault (see Figs. 1 and 2). Thus, we can use the fold faces to estimate the underlying fault dip direction.

3.2 Factors that affect overburden folding

Overburden folding induced by earthquakes is controlled by many factors, such as mechanical material properties, fault geometry, the tectonic stress field, etc. In this paper, only the overburden thickness, elastic properties (Young's modulus and Poisson's ratio), and fault dip angle are discussed.

Given a fixed fault dip angle of 30°, the effects of overburden thicknesses of 10 m, 100 m, and 500 m are shown in Fig. 3 for a fixed Young's modulus of 212 MPa and a Poisson's ratio of 0.40 in the overlying layer.

The magnitudes of the horizontal displacements in the models with different overburden thicknesses are smaller than those without overburden at the ground surface. Additionally, the thicker the overburden is, the smaller the horizontal displacement. Notably, the vertical displacements in models with overburden are larger than those without overburden, and the thinner the overburden is, the steeper the fold slope. The distances of the maximum horizontal and vertical displacements from Point A (in Fig. 1) increase and the fold height decreases with increasing overburden thickness. Figure 3(b) illustrates that the thicker the overburden is, the flatter the fold. Therefore, if a fold can be easily identified with the naked eye, the overburden is likely shallow. The effects of overburden discussed above are consistent with those noted in previous studies (Oglesby et al., 1998; Papadimitriou et al., 2007).

The effects of the mechanical material parameters of the overburden on the fold are illustrated in Fig. 4 for a fixed fault dip angle of 30° and an overburden of 80 m. The numerical results (Figs. 4(a) and 4(b)) show that the displacement and fold slope decreases as the Young's modulus value increases from 2.12 MPa (soil) to 212 MPa (sand) and 21.2 GPa (rocks). The differences in the displacements and fold slopes are not obvious for the first two orders of magnitude of Young's modulus (2.12 MPa and 212 MPa). Similarly, Figures 4(c) and 4(d) show the effects of Poisson's ratios of 0.34, 0.40, and 0.46 on the fold. These figures suggest that a larger Poisson's ratio leads to decreased horizontal displacement and increased

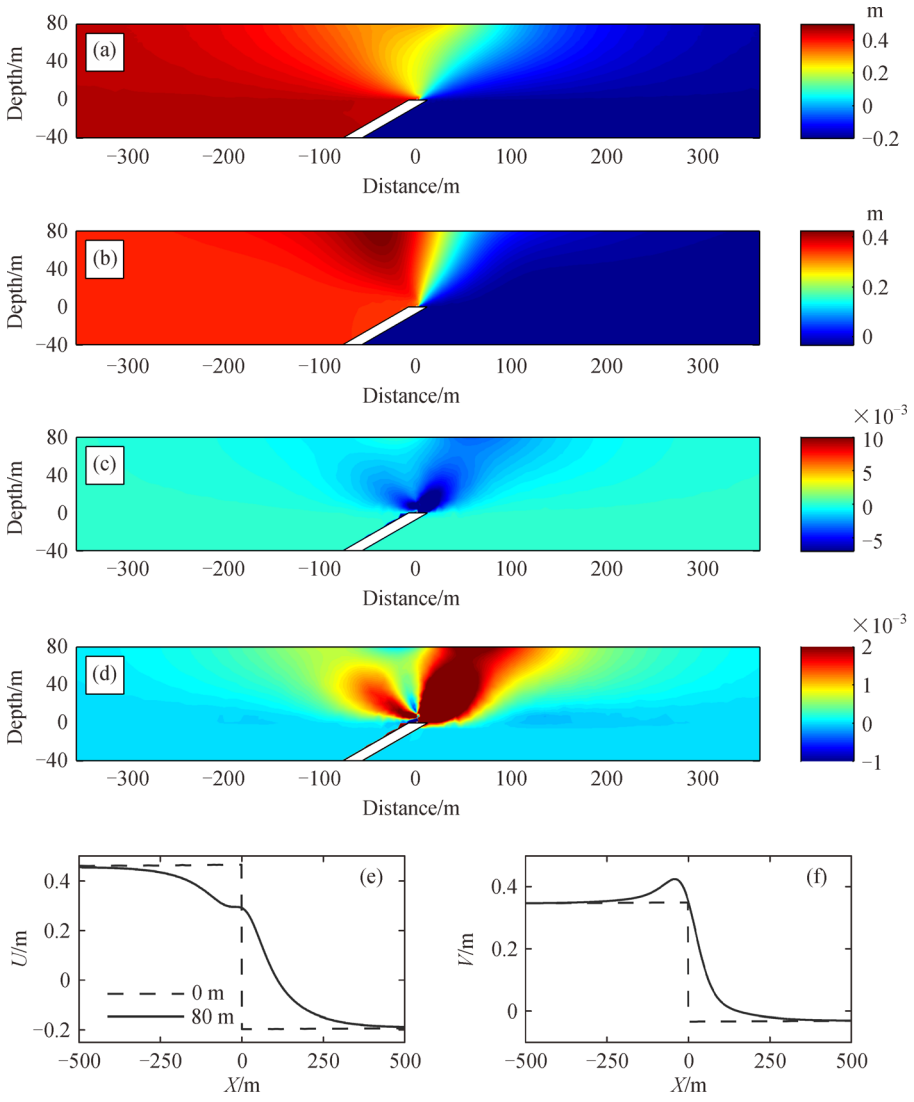

Fig. 2 Typical numerical results. (a)−(d) show the coseismic deformation and strain fields near the upper tip of the fault: (a) horizontal displacement field; (b) vertical displacement field; (c) and (d) horizontal and vertical strain fields (positive for extension), respectively; and (e) and (f) horizontal and vertical displacements at the ground surface, respectively. The dashed line represents the model without overburden, and the solid black line represents the model with 80 m of overburden.

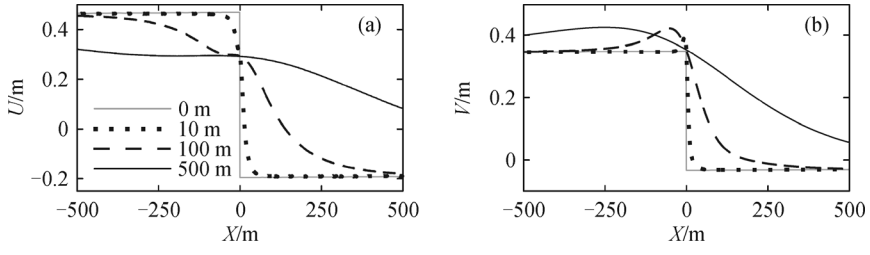

Fig. 3 Influence of overburden thickness on folding. (a) horizontal displacements; (b) vertical displacements.

fold height. The maximum vertical displacement (V_{max}) increases with increasing Poisson's ratio (Fig. 4(d)). Additionally, a larger Poisson's ratio results in the fold shifting closer to the fault, with a narrow deformation zone at the surface.

The displacements caused by thrust faults with different dip angles are shown in Fig. 5 for a fixed overburden depth of 80 m, a Young's modulus of 212 MPa, and a Poisson's ratio of 0.40. A significant change in the maximum vertical displacement can be observed at dip angles of 30° to 60°.

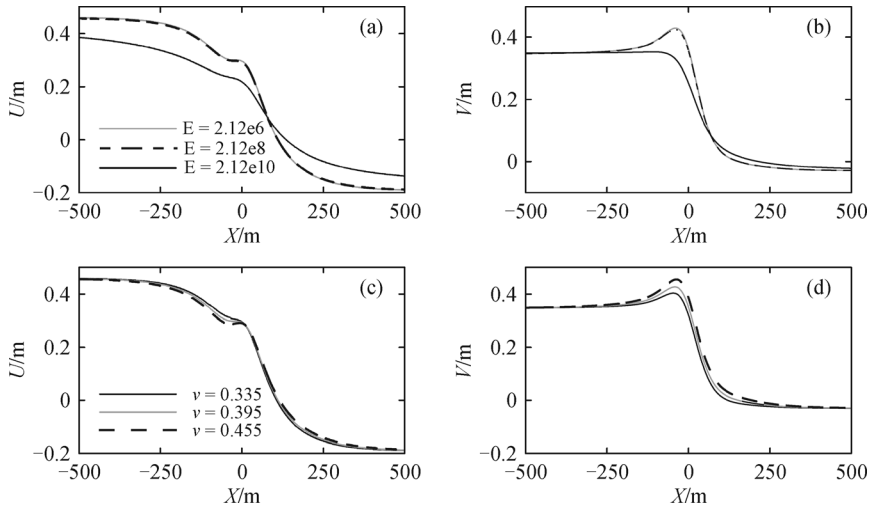

Fig. 4 Influence of mechanical parameters on overburden folds. (a) and (b) show the influence of Young's modulus. (c) and (d) show the influence of Poisson's ratio.

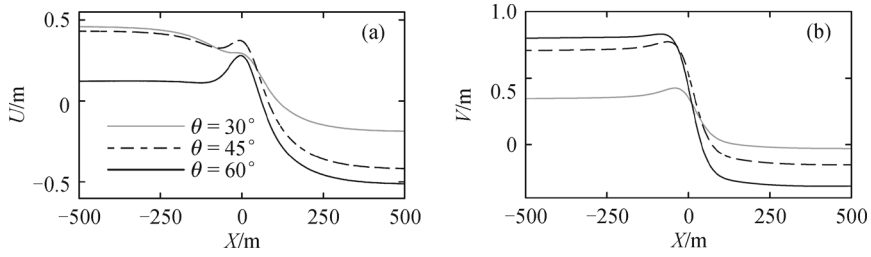

Fig. 5 Influence of fault dip angle. (a) horizontal displacements; (b) vertical displacements.

Additionally, the relative displacement increases to 98% as displacement varies from 0.42 m to 0.83 m, and the larger the dip angle is, the steeper the fold slope. These trends have also been observed in previous studies (Cole and Lade, 1984; Bray, 2001).

4 Case verification

The Wufeng excavation site (Lee et al., 2001; Yang et al., 2014) in Central Taiwan was used to investigate the deformation patterns in the soil sedimentary cover after the 1999 Chi-Chi event. The excavation site is approximately 10 m long and 4 m deep (Fig. 6(a)), and it is characterized by a continuous west-facing fault-related fold. Paleoseismic excavations (Lee et al., 2001; Yang et al., 2014) have identified Quaternary fluvial deposits that comprise the Wufeng trench wall, which overlies Pliocene bedrock. The deposits are approximately 8−10 m thick at the hanging wall (Fig. 6(b)). This depth supports the theory that an overburden layer is shallow if a fold can be easily identified by the naked eye. The dip angle of the west slope of the fold is larger than that of the east slope; thus, we can infer that the movement direction of the hanging wall is west based on the typical fold features noted previously.

Another issue is the prediction of fault slip using kinematic inversion for an earthquake with an overburden layer. The field survey (Lee et al., 2001; Yang et al., 2014) showed that the pop-up fold in Fig. 6(b) is 2.5 m high and that the thrust fault beneath the cover layer dips to the east at a dip angle of 34°. The fault slip occurred approximately 4±0.2 m from the excavation. This distance is shorter than the 4.47 m distance that was directly estimated from the fold height and fault dip considering the fault rupture reaches to the surface (Lee et al., 2001). This result suggests that fault slip inversion must consider the effect of the overburden layer. Our results show that fault slip based directly on patterns of uplift above fault-related scarps or folds may be inappropriate when fault ruptures stop in the sediments and do not reach the surface.

5 Conclusions

In this study, we proposed a conceptual model with a blind thrust fault zone and heterogeneous materials to simulate the coseismic features of surface deformation associated

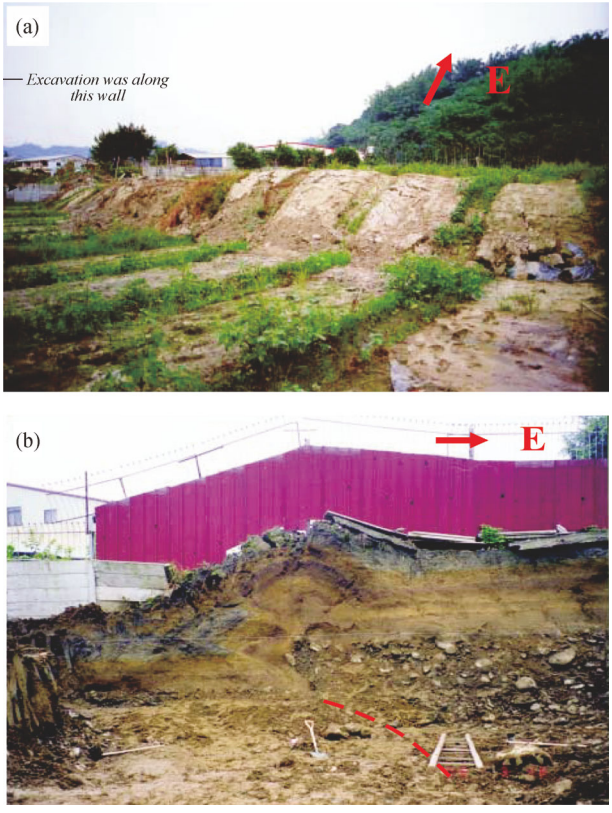

Fig. 6 Photographs of fault-related folding at the Wufeng excavation site. (a) The west-facing fault-related fold in the paddy field. (b) A cross-section of the Wufeng excavation site. The red dashed line is the main fault slip of the 1999 Chi-Chi earthquake (Mw = 7.6) that occurred in Central Taiwan (Lee et al., 2001; Yang et al., 2014).

with overburden layers of different thicknesses. This model is different from the dislocation model, which is based on the homogeneous half space and widely used in seismology. The principal results are as follows:

1) The maximum vertical displacement at the ground surface induced by a thrust fault with an overburden layer is larger than that when no overburden layer is present; however, the maximum horizontal displacement of the former is less than that of the latter. This result suggests that coseismic overburden folds amplify vertical ground deformation (Figs. 3(a) and 3(b)).

2) A region of horizontal compression and vertical extension exists near the upper fault dip in the overburden, and it is favorable for the development of an overburden fold. In this strain state, the direction of the front slope of the overburden fold is opposite to that of the fault dip (Figs. 2(e) and 2(f)). The dip angle of the front slope is larger than that of the back slope, and the front slope can be used to identify the face direction of the hanging wall.

3) The larger the fault dip angle is, the steeper the coseismic overburden fold. Additionally, folds become more difficult to identify in field surveys as the overburden thickness increases because the folds flatten and their heights do not change significantly. Therefore, overburden folds that are easily identifiable with the naked eye generally indicate shallow overburden.

4) The mechanical parameters of the overburden layer have important impacts on ground deformation. The magnitudes of the horizontal and vertical displacements, as well as the fold height, decrease with increasing Young's modulus. A large Poisson's ratio may decrease the horizontal displacement and increase the fold height (Fig. 4).

5) The deformation results of the conceptual model suggest that the fault dip angle is the primary factor that controls the coseismic overburden fold. The second most important factor is the overburden thickness, and the least important are the mechanical parameters of the overburden.

The conceptual model is simple, and the results are preliminary. However, we believe that these results may improve our understanding of overburden folds and our ability to identify these folds in field surveys.

Acknowledgements We would like to thank the anonymous reviewers for their constructive comments. This research was funded by the National Natural Science Foundation of China (Grant No. 41474080).

References

Bernard S, Avouac J P, Dominguez S, Simoes M (2007). Kinematics of fault-related folding derived from a sandbox experiment. Journal of Geophysical Research, 112(B3): B03S12

Brandes C, Tanner D C (2014). Fault-related folding: a review of kinematic models and their application. Earth Sci Rev, 138: 352–370

Bray J D (2001). Developing mitigation measures for the hazards associated with earthquake surface fault rupture. Seismic Fault-induced Failures: 55–80

Chen G H, Xu X W, Zheng R Z, Yu G H, Li F, Li C X, Wen X Z, He Y L, Ye Y Q, Chen X C, Wang Z C (2008). Quantitative analysis of the co-seismic surface rupture of the 2008 Wenchuan earthquake, Sichuan, China along the Beichuan-Yingxiu fault. Dizhen Dizhi, 30(3): 723–738 (in Chinese)

Cole D A Jr, Lade P V (1984). Influence zones in alluvium over dip-slip faults. J Geotech Eng, 110(5): 599–615

Donald L T, Gerald S (2001). Geodynamics (2nd ed). Cambridge: Cambridge University Press, 78

Galuppo C, Toscani G, Turrini C, Bonini L, Seno S (2016). Fracture patterns evolution in sandbox fault-related anticlines. Italian Journal of Geoscience, 135(1): 5–16

Gudmundsson A (2004). Effect of Young's modulus on fault displacement. C R Geosci, 336(1): 85–92

Hardy S, Finch E (2006). Discrete element modeling of the influence of cover strength on basement-involved fault-propagation folding. Tectonophysics, 415(1−4): 225–238

Hu C B, Zhou Y J, Cai Y E, Wang C Y (2009). Study of earthquake triggering in a heterogeneous crust using a new finite element model.

Seismol Res Lett, 80(5): 799–807

Hubert-Ferrari A, Suppe J, Gonzalez-MieresR, Wang X (2007). Mechanisms of active folding of the landscape (southern Tian Shan, China). Journal of Geophysical Reseach, 112(B3): B03S09

Hughes A N, Benesh N P, Shaw J H (2014). Factors that control the development of fault-bend versus faultpropagation folds: insights from mechanical models based on the discrete element method (DEM). J Struct Geol, 68: 121–141

Ishiyama T, Sato H, Kato N, Nakayama T, Iwasaki T, Abe S (2011). Structures of active blind thrusts beneath Tokyo Metropolitan area. AGU Fall Meeting 2011, abstract T54B-02

Johnson K M, Johnson A M (2002). Mechanical models of trishear-like folds. Journal of Structure Geology, 24(2): 277–287

Lee J C, Chen Y G, Sieh K, Mueller K, Chen W S, Chu H T, Chan Y C, Rubin C, Yeats R (2001).A vertical exposure of the 1999 surface rupture of the Chelungpu Fault at WuFeng, Western Taiwan: structural and paleoseismic implications for an active thrust fault. Bulletin of the Seismological Society of America, 91(5): 914–929

Lewis M M, Jackson C A L, Gawthorpe R L (2013). Salt-influenced normal fault growth and forced folding: the Stavanger Fault System, North Sea. J Struct Geol, 54: 156–173

Lin J, Stein R (1989). Coseismic folding, earthquake recurrence, and the 1987 source mechanism at Whittier Narrows, Los Angeles Basin, California. J Geophys Res, 94(B7): 9614–9632

Miller R D, Xia J (1998). Large near-surface velocity gradients on shallow seismic reflection data. Geophysics, 63(4): 1348–1356

Oglesby D D, Archuleta R J, Nielsen S B (1998). Earthquakes on dipping faults: the effects of broken symmetry. Science, 280(5366): 1055–1059

Papadimitriou A, Loukidis D, Bouckovalas G, Karamitros D (2007). Zone of excessive ground surface distortion due to dip-slip fault rupture. 4th International Conference on Earthquake Geotechnical Engineering, Paper No.1583

Qayyum M, Spratt D A, Dixon J M, Lawrence R D (2015). Displacement transfer from fault-bend to fault-propagation fold geometry: an example from the Himalayan thrust front. J Struct Geol, 77: 260–276

Roering J J, Cooke M L, Pollard D D (1997). Why blind thrust faults do not propagate to the Earth's surface: numerical modeling of coseismic deformation associated with thrust-related anticlines. Journal of Geophysical Reseach, 102(B6 B2): 11901–11912

Shaw J H, Shearer P M (1999). An elusive blind-thrust fault beneath metropolitan Los Angeles. Science, 283(5407): 1516–1518

Shaw J H, Suppe J (1996). Earthquake hazards of active blind-thrust faults under the central Los Angeles basin, California. J Geophys Res, 101(B4): 8623–8642

Shi C X (1994). Materials Comprehensive Dictionary. Beijing: Chemical Industry Press (in Chinese)

Suppe J (1983). Geometry and kinematics of fault-bend folding. Am J Sci, 283(7): 684–721

Suppe J, Chou G T, Hook S C (1992). Rates of folding and faulting determined from growth strata. Thrust Tectonics, 105–121 doi: 10.1007/978-94-011-3066-0_9

Turko J M, Knuepfer P L K (1991). Late Quaternary fault segmentation from analysis of scarp morphology. Geology, 19(7): 718–721

Walker R T, Khatib M M, Bahroudi A, Rodés A, Schnabel C, Fattahi M, Talebian M, Bergman E (2015). Co-seismic, geomorphic, and geologic fold growth associated with the 1978 Tabas-e-Golshan earthquake fault in eastern Iran. Geomorphology, 237: 98–118

Yu G, Xu X, Klinger Y, Diao G, Chen G, Feng X, Li C, Zhu A, Yuan R, Guo T, Sun X, Tan X, An Y (2010). Fault-scarp features and cascading-rupture model for the *M*w 7.9 Wenchuan Earthquake, Eastern Tibetan Plateau, China. Bull Seismol Soc Am, 100(5B): 2590–2614

Xu X W, Wen X Z, Han Z J, Chen G H, Li C Y, Zheng W J, Zhnag S M, Ren Z Q, Xu C, Tan X B, Wei Z Y, Wang M M, Ren J J, He Z T, Liang M J (2013). Lushan *Ms*7.0 earthquake: a blind reserve-fault event. Chin Sci Bull, 58(28−29): 3437–3443

Yang J L, Ilic J G, Wardlaw T (2003). Relationships between static and dynamic moduli of elasticity for a mixture of clear and decayed eucalypt wood. Aust For, 66(3): 193–196

Yang Y R, Hu J C, Lin M L (2014). Evolution of coseismic fault-related folds induced by the Chi-Chi earthquake: a case study of the Wufeng site, Central Taiwan by using 2D distinct element modeling. J Asian Earth Sci, 79: 130–143

Zhou Y J, Hu C B, Cai Y E (2009). Influence of an inhomogeneous stress field and fault-zone thickness on the displacements and stresses induced by normal faulting. J Struct Geol, 31(5): 491–497

Zuluaga L F, Fossen H, Rotevatn A (2014). Progressive evolution of deformation band populations during Laramide fault-propagation folding: Navajo Sandstone, San Rafael monocline, Utah, U.S.A. Journal of Structural Geology, 68: 66–81